

Privacy Protection Framework against Unauthorized Sensing in the 5.8 GHz ISM Band

Zexin Fang*, Bin Han*, and Hans D. Schotten*[†]

*University of Kaiserslautern (RPTU), Germany

[†]German Research Center for Artificial Intelligence (DFKI), Germany

Abstract—Unauthorized sensing activities pose an increasing threat to individual privacy, particularly in the industrial, scientific, and medical (ISM) band where regulatory frameworks remain limited. This paper presents a novel signal process methodology to monitor and counter unauthorized sensing activities. Specifically, we model the pedestrian trajectories as a random process. Then, we leverage the Cramér-Rao bound (CRB) to evaluate sensing performance and model it as sampling error of such a random process. Through simulation, we verify the accuracy of monitoring unauthorized sensing activities in urban scenarios, and validate the effectiveness of corresponding mitigation strategies.

Index Terms—Privacy, radio sensing, tracking, CRB.

I. INTRODUCTION

With the rapid advancement of sensing systems, environmental modeling, and data analysis techniques, our world is becoming increasingly monitored and interconnected. These technological developments offer significant benefits for automation, safety, and efficiency across various domains [1], [2]. As data collection becomes increasingly pervasive, while numerous studies propose privacy-preserving frameworks for sensing data sharing [3] or encryption [4], the critical risk of data acquisition through unauthorized sensing systems remains largely unexplored. Meanwhile, regulatory frameworks addressing this issue are currently absent, they are urgently needed at both international and national levels. Legitimate sensing systems can embed authentication watermarks in their waveforms upon certification by authorized organizations, following approaches like [5]. Consequently, the primary concern shifts to unauthorized sensing systems, particularly those operating in industrial, scientific, and medical (ISM) bands, since unauthorized sensing in licensed bands already faces legal consequences under current spectrum allocation regulations. To monitor such sensing activities, we present a novel methodology from a signal process perspective. Specifically, we model pedestrian trajectories as a random process, where unauthorized sensing acts as sampling of this process. Combined with environmental modeling, this enables unauthorized initiators to analyze individual behaviors. Notably, large sampling errors usually lead to misinterpretation of individual behaviors. Therefore, the key of preserving individual privacy against unauthorized sensing systems lies in monitoring sampling errors and interfering with sensing systems when necessary.

The sampling error of a sensing system depends on waveforms, channel conditions, and sensing initiator configurations,

making it challenging to estimate the actual sensing performance from the target's perspective. Therefore, we use the Cramér-Rao bound (CRB) of sensing capacity to represent the achievable minimum error in a sensing system. In Sec. II, and more specifically in Sec. II-A and Sec. II-C, we describe all the potential errors of the sensing system. In Sec. III-A, we model the sensing error as sampling error to characterize the tracking performance of the sensing initiator. In Sec. III, we conduct simulations to validate the feasibility of accessing the CRB when waveforms are distorted by channel effects. More importantly, we compare the estimated CRB with the actual CRB of the sensing initiator. Based on these simulation results, we propose and validate corresponding mitigation strategies. In Sec. IV, we conclude this paper.

II. SYSTEM MODEL

A. CRB of sensing resolution

In radar waveform design, the ambiguity function (AF) specifies the output of a matched filter in the absence of noise. It is generally used to evaluate the performance of radar waveforms. The AF of a discrete signal can be described,

$$\mathcal{A}(k, f_v) = \sum_{n=1}^N \left| s[n]s^*[n+k]e^{j2\pi\frac{f_v n}{NT}} \right|, \quad (1)$$

where v, k correspond to the Doppler shift and bit time delay, and T represents the sample interval. A common method for estimating radar waveform sensing resolution involves determining the point where power drops by 3 dB from its peak in the AF. However, this approach is computationally intensive for constant monitoring; therefore, we directly access the CRB of sensing pulses. The Fisher information matrix (FIM), which quantifies parameter estimation precision from observations, is given in [6]:

$$\mathbf{J}_M(k, f_v) = -2\gamma \begin{bmatrix} \frac{\partial^2 \mathcal{A}(k, f_v)}{\partial^2 k} & \frac{\partial^2 \mathcal{A}(k, f_v)}{\partial k \partial f_v} \\ \frac{\partial^2 \mathcal{A}(k, f_v)}{\partial k \partial f_v} & \frac{\partial^2 \mathcal{A}(k, f_v)}{\partial^2 f_v} \end{bmatrix} \Bigg|_{\substack{k=0 \\ f_v=0}}, \quad (2)$$

where γ is the signal to noise ratio (SNR) of sensing pulses.

In a monostatic sensing configuration, depicted in Fig. 1, the delay of signal and frequency shift can be then described as follows:

$$k = \frac{2D}{c}, \quad (3)$$

$$f_v = \frac{2f_c \cos(\phi + \theta)V}{c}, \quad (4)$$

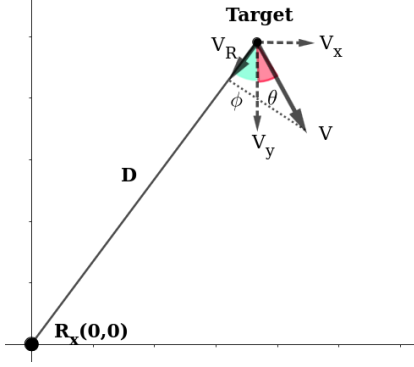


Fig. 1: Monostatic sensing geometry

where D is the distance between the sensing initiator and the target, c denotes the speed of light, f_s represents the sampling frequency, and f_c is the carrier frequency of the sensing signal. Additionally, V is the velocity of the target, ϕ is the look angle from the receiver, and θ represents the vertical angle of the target's velocity. The radial velocity component is given by $V_R = \cos(\phi + \theta)V$. Then, the FIM can be reformulated as a function of D and V_R :

$$\mathbf{J}_M(D, V_R) = -2\gamma \begin{bmatrix} \frac{\partial^2 \mathcal{A}(D, V_R)}{\partial D^2} & \frac{\partial^2 \mathcal{A}(D, V_R)}{\partial D \partial V_R} \\ \frac{\partial^2 \mathcal{A}(D, V_R)}{\partial D \partial V_R} & \frac{\partial^2 \mathcal{A}(D, V_R)}{\partial V_R^2} \end{bmatrix}_{\substack{D=0 \\ V_R=0}} \quad (5)$$

Applying the chain rule we can get

$$-\frac{\partial \mathcal{A}^2(D, V_R)}{\partial D^2} \Big|_{\substack{D=0 \\ V_R=0}} = \frac{4f_s^2}{T^2 c^2} \sum_{n=1}^N |s[n] - s[n-1]|^2, \quad (6)$$

$$-\frac{\partial \mathcal{A}^2(D, V_R)}{\partial V_R^2} \Big|_{\substack{D=0 \\ V_R=0}} = \frac{16\pi^2 f_c^2}{c^2 N^2} \sum_{n=1}^N n^2 |s[n]|^2, \quad (7)$$

$$-\frac{\partial \mathcal{A}^2(D, V_R)}{\partial k \partial V_R} \Big|_{\substack{D=0 \\ V_R=0}} = -\Im \left\{ \frac{8f_s f_c \pi}{c^2 N T} \sum_{n=1}^N n (s[n] - s[n-1]) s^*[n] \right\}. \quad (8)$$

The CRB can be defined as follows:

$$\text{CRB}(D) = [\mathbf{J}_M^{-1}(D, V_R)]_{[1,1]} \quad (9)$$

$$\text{CRB}(V_R) = [\mathbf{J}_M^{-1}(D, V_R)]_{[2,2]} \quad (10)$$

The square root of $\text{CRB}(D)$ and $\text{CRB}(V_R)$ represents the minimum possible variance in measuring D and V_R . On the other hand, direction of arrival (DOA) estimation depends on neither directly. Instead, its lower bound is a monotonically decreasing function of SNR, as shown in [7]. For simplicity, we use a fixed lower bound to represent the angle estimation error, as the $\text{CRB}(\theta)$ is typically small and not the primary focus of this paper.

As introduced in Sec. I, the spatial information of a pedestrian can be modeled as a random process $\mathbf{m}(t)$, where the trajectory and related quantities evolve over time. Each

individual measurement of this process can be interpreted as a discrete sample drawn from the underlying random process. To represent the spatial information measured at the k_{th} time step, we define the corresponding vectors: $\mathbf{m}(k) = [D^k, V_R^k, \phi^k]^T$, $\mathbf{e}(k) = [e_D^k, e_{V_R}^k, e_\phi^k]^T$. Meanwhile, $\mathbf{m}(k)$ can be expressed as:

$$e_D^k \sim \mathcal{N}(0, \sigma_D^2), \quad \sigma_D = \sqrt{\text{CRLB}(D)}; \quad (11)$$

$$e_{V_R}^k \sim \mathcal{N}(0, \sigma_{V_R}^2), \quad \sigma_{V_R} = \sqrt{\text{CRLB}(V_R)}; \quad (12)$$

$$e_\phi^k \sim \mathcal{N}(0, \sigma_\phi^2), \quad \sigma_\phi = \sqrt{\text{CRLB}(\phi)}. \quad (13)$$

B. Error model of data association

Unauthorized sensing frequently encounters frequency and bandwidth constraints, alongside interference from various signals. In indoor and urban settings, sensing is further complicated by clutter from walls, buildings, and diverse objects. These obstacles can lead to distorted readings, particularly when tracking slow-moving targets like pedestrians, given the inherently limited velocity resolution of unauthorized sensing systems. Some studies have demonstrated the ability to differentiate between pedestrians, cyclists, and vehicles using micro-Doppler signatures [8]. However, these works also emphasize the significant challenge posed by noisy micro-Doppler signatures. Another common method for data association is the joint probability data association (JPDA) algorithm. JPDA prunes infeasible hypotheses and calculates the most probable ones [9]. Given the constraints of limited sensing performance, slowly moving targets, and highly cluttered environments, the efficacy of this approach remains to be fully validated. Drawing from these insights, we can postulate from the unauthorized sensing perspective: at any given moment, there exists a probability that the target's spatial information is not to be retrieved. While the interference and noise of the sensing initiator cannot be modeled, we can represent this uncertainty through two key factors: the target's radial velocity V_R and the velocity resolution. The probability density function of measuring V_R of the moving target can be described as:

$$P_t(V_R, \sigma_{V_R}) = \frac{1}{\sqrt{2\pi}\sigma_{V_R}} \exp\left(-\frac{(\dot{V}_R - V_R)^2}{2\sigma_{V_R}^2}\right). \quad (14)$$

The cumulative difference of measuring static clutters and a moving target can be written in terms of the error function as $p_k = \text{erf}\left(\frac{V_R}{\sqrt{2}\sigma_{V_R}}\right)$, which can also be extended while multiple targets exist. We define a sample function $\delta(k)$ to denote whether a valid sample of $\mathbf{m}(t)$ can be obtained:

$$\delta_k(k) = \begin{cases} 1 & \text{with probability } p_k, \\ 0 & \text{with probability } 1 - p_k. \end{cases} \quad (15)$$

The sampled spatial information for a single target is then

$$\mathbf{m}_\sigma(k) = \sum_{k=1}^K (\mathbf{m}(k) + \mathbf{e}(k)) \delta(k). \quad (16)$$

C. Error model of tracking performance

In a monostatic sensing scenario, the orientation of the target velocity usually can not be directly solved [10]. As depicted in Fig. 1, the actual target velocity V relates to radial velocity V_R by $V = \frac{V_R}{\cos(\phi+\theta)}$, where ϕ is known and θ is unknown (Fig. 1). We simplify tracking by omitting velocity estimation, as V measurements are too noisy and uncertain for standard Kalman filtering. Using the cosine principle, the true position deviation between $\hat{\mathbf{m}}(k)$ and $\mathbf{m}(k)$ can be quantified as $|\Delta_D(k)|$, where

$$\begin{aligned} |\Delta_D(k)| &= \sqrt{(D^k + e_D^k)^2 + (D^k)^2 - 2D^k(D^k + e_D^k) \cos e_\phi^k} \\ &= \sqrt{2(D^k + e_D^k)(1 - \cos e_\phi^k) + (e_D^k)^2} \end{aligned} \quad (17)$$

The true position deviation $|\Delta_D(k)|$ can be assigned a sign based on the polarity of e_D^k , allowing it to be modeled as Gaussian distributed: $\Delta_D(k) \sim \mathcal{N}(0, \sigma_M^k)$. Simulation results indicate that the impact of D^k on σ_M^k is negligible when compared to the effects of σ_D^k or σ_ϕ^k .

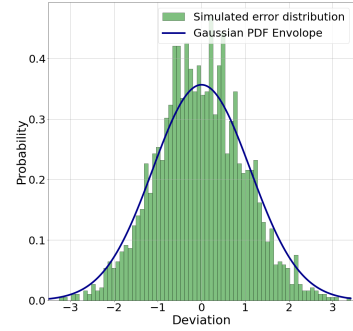
As introduced earlier, the target periodically measures the sensing capacity of the received signal. The sensing capacity is characterized by the probability that the sensing initiator retrieves a valid measurement within a time interval Δt . For a longer interval $\Delta T = K \Delta t$, the actual number of valid measurements \tilde{n} satisfies $\tilde{k} \leq K$. Therefore, the tracking error can be evaluated in terms of the quantization error of this random process, depicted in Fig. 3. The average quantization interval can be determined by $\Delta q = \frac{K \Delta t}{\sum_{k=1}^K p_k}$. With

$\Delta q|_{K=1} = \frac{\Delta t}{p_1}$, the quantization error for data association is $\sigma_q^k = \frac{\Delta t^2}{12 p_k^2}$, derived from $\sigma_q = \frac{\Delta q^2}{12}$. Taking all possible errors into account, the performance lower bound can be expressed as a signal sampling error: $\sigma_p^k = \sigma_M^k + \sigma_q^k$, where σ_M^k can be regarded as the signal noise power.

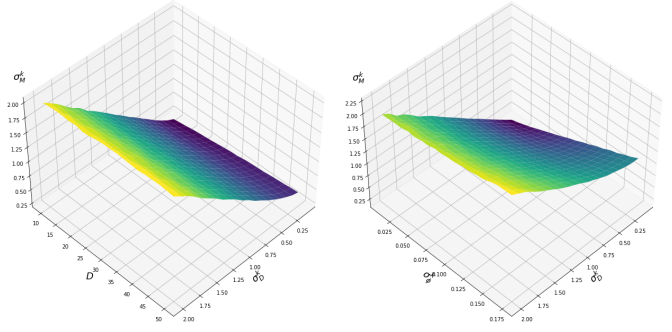
III. SIMULATION

A. Sensing components assessment

The sensing initiator typically transmits multiple pulses within an update interval to enhance the SNR of the reflected signals from the target. These pulses are usually short in time, suited for short-range sensing applications. However, in urban or indoor environments, the received signal power can be significantly attenuated, and the signal is particularly susceptible to interference, especially in the ISM band where multiple devices coexist. Due to the high correlation between sensing pulses, the signal periodicity can be estimated by cross-correlating a short segment of the received signal with a slightly longer segment. After identifying the periodicity, shifted summation is performed to enhance the SNR. The detailed implementation is presented in Algorithm 1. One concern arises from miss-detection of communication signals. While these signals can be highly correlated, they typically operate at lower power than sensing requires. Nevertheless, their distinctly higher CRB makes them distinguishable and prevents triggering the mitigation strategies proposed in the following section.



(a) Simulated error compared to Gaussian PDF



(b) σ_M^k w.r.t. D^k and σ_ϕ^k

(c) σ_M^k w.r.t. D^k and σ_D^k

Fig. 2: Error w.r.t. D^k , σ_ϕ^k and σ_D^k

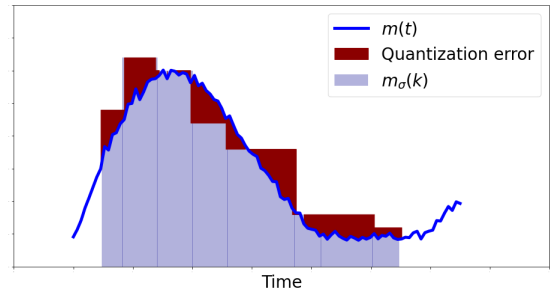


Fig. 3: Error of non-uniform quantization

After isolating the periodical component, we can use it to estimate $\text{CRB}(D)$ and $\text{CRB}(V_R)$. We define the target-estimated CRB as CRB_T , and the actual CRB from the sensing initiator as CRB_I . The key distinctions between CRB_T and CRB_I are that the target lacks knowledge of the reflected SNR in relation to the sensing initiator, and the actual sensing pulses are subject to noise and fading. Unlike conventional communication systems that use pilot signals for channel estimation to mitigate fading, blind channel estimation can be done without pilots but involves high computational complexity [11].

To investigate the impact of fading channels, we evaluated the CRB_I and CRB_T through numerical simulations under different channel conditions. We considered three scenarios: additive white Gaussian noise (AWGN) channel, Rayleigh fading channel, and Rician fading channel with a K-factor of 2. Besides, we consider equally powered noise and orthogonal frequency-division multiplexing (OFDM) symbols as noise

Algorithm 1: correlation-based sensing components extraction (CSCE)

```

1 Input: received signal in a single assessment interval  $r(n)$ ; short signal
  segment length  $N_s$  and long signal segment length  $N_l$ 
2 Output: the sensing pulse  $p$ 
3 Function CSCE :
4   slice the received signal  $r(n)$  with length  $N_s$  and  $N_l$  as  $r_s$  and  $r_k$ 
5    $k = 0, 1, 2, \dots, N_s + N_l - 2$ 
6    $C(k) = \sum_{l=1}^{N_l} r_s(l)r_k^*(l - k + N_l - 1)$ 
7    $C(k) = \frac{C(k)}{\max(C(k))}$ 
8    $I \leftarrow \{k : C(k) \text{ satisfies } C(k) > 0.707\}$ 
9   // indices where the correlation is high
10   $\Delta = \{I(i+1) - I(i) : i \in \{1, \dots, |I| - 1\}\}$ 
11  // the difference of indices
12   $N_p = |\{d \in \Delta : d \geq 0.4 \max(\Delta)\}|$ 
13  // filter out closely located indices
14   $L = \left\lfloor \frac{\sum_{i=1}^{N_p} \Delta_i}{N_p} \right\rfloor$ 
15   $N_{all} = \frac{|r(n)|}{T_{period}}; s(l) = \sum_{j=1}^{N_{all}} r(n - jL)$ 
16  // Shifted summation
17   $h(l) = \frac{1}{100}; s_{ma}(l) = s(l) * h(l)$ 
18  // moving average
19   $l_{start} = \min\{l : s_{ma}(l) \geq 0.707 \cdot \max(s_{ma})\}$ 
20   $l_{end} = \max\{l : s_{ma}(l) \geq 0.707 \cdot \max(s_{ma})\}$ 
21  // locate the sensing pulse
22   $p = s(l)$  for  $l_{start} \leq l \leq l_{end}$ 
23 end

```

TABLE I: Sensing pulse description

	Parameter	Value	Remark
LFM	B	100 Mhz	Bandwidth
	f_c	5.8 Ghz	Carrier Frequency
	T_p	0.1 ms	Pulse Duration
	PRT	0.4 ms	Pulse Repetition Time

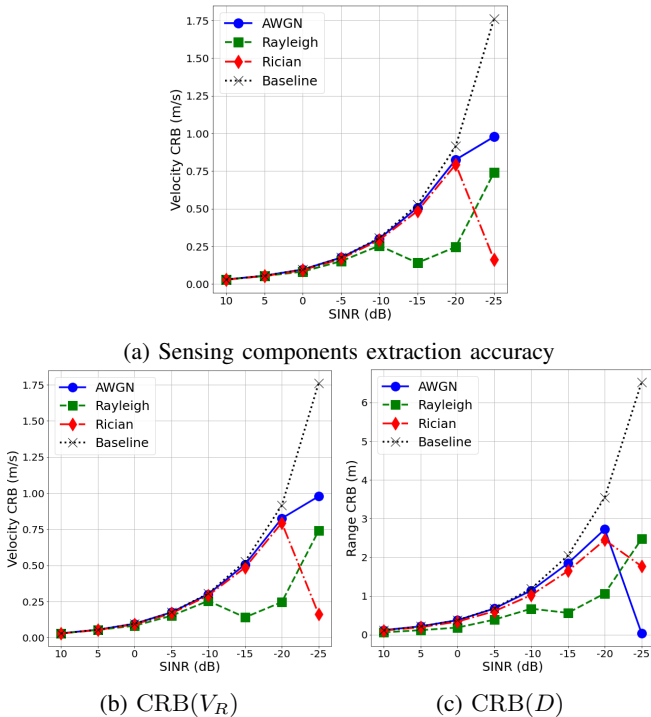


Fig. 4: CRB(V_R), CRB(D) estimation and CSCE accuracy under different channel response.

and interference background. The sensing pulse is detailed in Table I. We use linear frequency modulation (LFM) pulses, as they are commonly employed to achieve high range resolution in short-range sensing applications through pulse compression techniques [12]. The CRB was then calculated using signal segments of 0.05 sec. The simulation results are presented in Fig. 4. As shown in Fig. 4a, under Rayleigh fading, when SINR drops below -10 dB, CSCE fails to detect sensing components, hence the estimated CRB cannot track the noise- and interference-free baseline (CRB₁). Meanwhile, such cutoff point exists when SINR drops below -20 dB under AWGN and Rician fading. The Rayleigh fading channel introduces severe inter-symbol interference (ISI), making sensing pulse detection more challenging. The ISI combined with noise results in estimated CRB values consistently below baseline, as evident in Figs. 4b- 4c, where *Baseline* > *AWGN* > *Rician* > *Rayleigh* generally holds. These results indicate that the CRB may not be assessed when the SINR falls below -10 dB. Since reflected signals are significantly weaker than the target received signal, such weak signals become infeasible for sensing purposes. Thus, the risk of being unable to access the CRB during actual sensing can be ignored.

B. Sensing activities detection and mitigation

After evaluating the accuracy of the CRB in the previous subsection, we proceed to conduct further simulations that account for mobility and urban environments. For the urban path loss channel, we consider the *3rd Generation Partnership Project* (3GPP) channel model under the *Canyon Street* scenario [13], examining both line of sight (LOS) and non-line of sight (NLOS) conditions. For LOS and NLOS,

$$L_{LOS} = 32.4 + 21 \log_{10}(d) + 20 \log_{10}(f_c) + X_{\sigma}; \quad (18)$$

$$X_{\sigma} \sim \mathcal{N}(0, 4),$$

$$L_{NLOS} = 35.3 \log_{10}(d) + 22.4 + 21.3 \log_{10}(f_c) - 0.3(h - 1.5) + X_{\sigma}; \quad (19)$$

$$X_{\sigma} \sim \mathcal{N}(0, 7.82).$$

Where d denotes the distance between the transmitter and receiver. For pedestrians on the ground, we assume a height of 1.5 m. To simplify calculation of reflected signal path loss, we approximate it by using twice the direct distance, neglecting signal absorption effects. The channel response is then modeled using Rayleigh fading for NLOS conditions and Rician fading for LOS conditions.

For mobility modeling of a pedestrian, we consider an average walking speed of 1.4 m/s with directional movements subject to confined randomness. The constrained random trajectory of a pedestrian's movement pattern is illustrated in Fig. 5. As the pedestrian moves through the urban environment, the channel conditions alternate between LOS and NLOS, simulating realistic radio propagation characteristics. Since reflected signals are weaker than those received directly by the target, we compensate by adding β_r to the estimated SINR, where β_r is derived from the average difference between Eqs. (18) and (19) at distances of 25 m and 50 m.

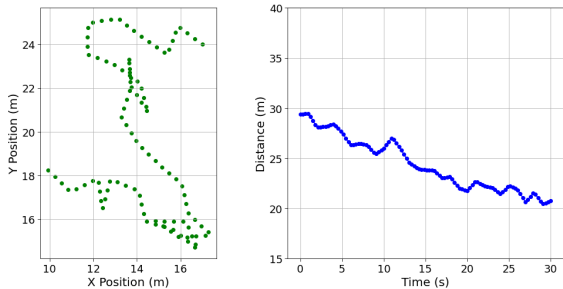


Fig. 5: Randomly generated trajectory

TABLE II: Simulation Setup I

	Parameter	Value	Remark
System	B	50, 150 Mhz	Bandwidth
	T_r	15 dBm	Transmitting power
	N_f	-92 dBm	Noise floor in ISM band [14]
	CRB(ϕ)	0.02 rad	Angle estimation lower bound
	β_r	-6 dB	Compensation factor for reflection

Simulations were conducted across two bandwidths using the parameters in Tab. II, assuming negligible external interference. Fig. 6 shows the results, with the performance lower bound (Sec. II-C) depicted as a shaded region around $\mathbf{m}(t)$. The results show that performance lower bounds are more accurately described when they are small. The average actual lower bounds for two bandwidths are 0.20 m and 0.43 m, compared to estimated values of 0.17 m and 0.24 m. This discrepancy arises because signals with larger bandwidths are more robust to multi-path effects.

While the performance lower bound can be estimated, the target can protect its privacy by transmitting noise pulses in the direction of incoming sensing signals, thereby decreasing the SNR for the sensing initiator's receiver. Even with perfect jamming power estimation by the sensing initiator, distance estimation based on received jamming power remains highly unreliable due to severe path loss fluctuations. Meanwhile, the transmission jamming power can be further randomized to mitigate this risk. Accordingly, we define two different monitoring strategies below to regulate the conditions under which jamming mode will be triggered.

1) *Strategy I: Instant Monitoring:*

Step 1: Monitor performance lower bound $\sigma_p(k)$. When $\sigma_p(t) < \theta_p$, increment J_{count} .

Step 2: When J_{count} reaches θ_J , activate jamming mode: transmit noise pulse with length L_j and power P_j , then reset J_{count} .

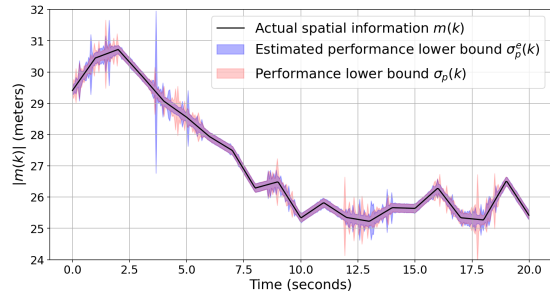
Step 3: Return to **Step 1** after transmission.

2) *Strategy II: Moving Average Monitoring:*

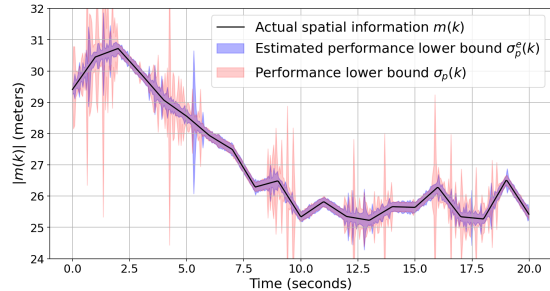
Step 1: Monitor performance lower bound $\sigma_p(k)$. Calculate moving average $\bar{\sigma}_p = \frac{1}{K_m} \sum_{i=k-K_m+1}^k \sigma_p(k)$. When $\bar{\sigma}_p < \theta_p$, increment J_{count}

Steps 2 & 3: same as *Strategy I*.

We validate the proposed monitoring strategies against unauthorized sensing systems through simulations using two sens-



(a) 150 Mhz bandwidth



(b) 50 Mhz bandwidth

Fig. 6: Performance lower bound of LFM pulses with three different bandwidths

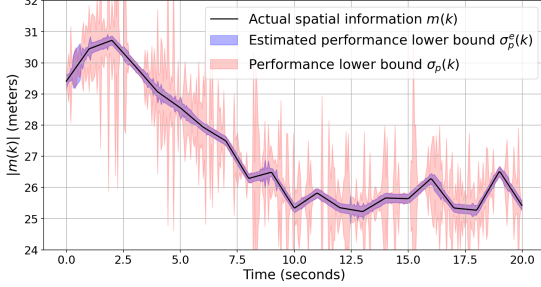
ing pulses with bandwidths of 50 MHz and 150 MHz. The jamming noise power is set as $P_j = a_j P_r$, where P_r denotes the received sensing signal power at the target, and other simulation parameters are listed in Tab. III. The simulation results, presented in Figs. 7 and 8, demonstrate a significant increase in $\sigma_p(k)$ when compared to the results shown in Fig. 6. This increase is particularly pronounced in the "smooth" regions of Fig. 6, where LOS exists between the target and sensing initiator. Quantitatively, under *Strategy I*, the mean of $\sigma_p(k)$ increased from 0.43 m to 0.78 m for 50 MHz bandwidth, and from 0.20 m to 0.33 m for 150 MHz bandwidth. Over 10 simulations, the jamming mode was triggered on average 35 times for 50 MHz bandwidth and 50 times for 150 MHz bandwidth. Under *Strategy II*, the mean of $\sigma_p(k)$ increased to 0.52 m for 50 MHz bandwidth signals and 0.32 m for 150 MHz bandwidth, with average trigger counts of 20 and 45 times, respectively. These simulation results show *Strategy I* achieves higher sensitivity and stronger interference with unauthorized sensing systems, though *Strategy II* triggers less frequently—particularly for 50 MHz bandwidth signals. Since 50 MHz bandwidth signals already exhibit large $\sigma_p(k)$, *Strategy II*'s reduced trigger frequency offers a more energy-efficient solution for mobile devices while maintaining effective monitoring performance.

IV. CONCLUSION

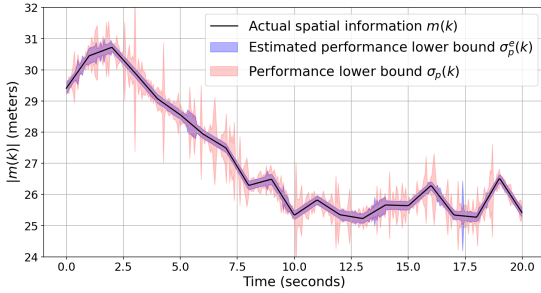
This paper presents a framework enabling individuals to monitor unauthorized sensing activities in ISM bands. We investigated accessing CRB in urban environments without computationally expensive blind channel estimation. The ac-

TABLE III: Simulation Setup II

	Parameter	Value	Remark
Mitigation	θ_p	0.17 m	Performance threshold
	θ_J	3	Count number threshold
	L_j	$\sim \mathcal{U}(50, 350)$ ms	Noise pulse duration
	a_j	$\sim \mathcal{U}(-3, 3)$ dB	Power modifier
	K_m	3	Steps of moving average

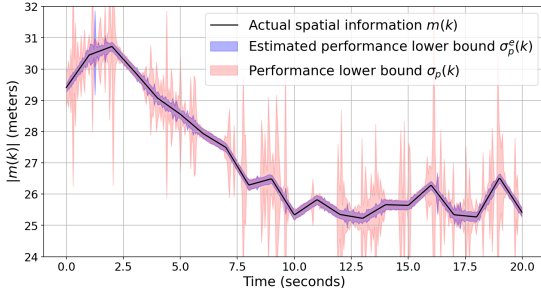


(a) 50 Mhz bandwidth

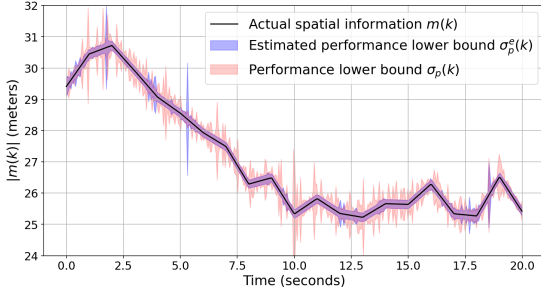


(b) 150 Mhz bandwidth

Fig. 7: Performance lower bound under *Strategy I*



(a) 50 Mhz bandwidth



(b) 150 Mhz bandwidth

Fig. 8: Performance lower bound under *Strategy II*

cessed CRB was modeled as a random process with sampling and quantization errors to characterize tracking accuracy of individuals. Next, we proposed and validated a jamming strategy that reduces tracking accuracy to preserve privacy. Given the proliferation of sensing techniques, this work offers crucial insights for preserving individual privacy in increasingly monitored environments.

ACKNOWLEDGMENT

This work is supported by the German Federal Ministry of Education and Research within the project Open6GHUB (16KISK003K/16KISK004). B. Han (bin.han@rptu.de) is the corresponding author.

REFERENCES

- [1] H. Huang *et al.*, “An integrated risk sensing system for geo-structural safety,” *J. Rock Mech. Geotech. Eng.*, vol. 9, no. 2, pp. 226–238, 2017.
- [2] H. Askari *et al.*, “Embedded self-powered sensing systems for smart vehicles and intelligent transportation,” *Nano Energy*, vol. 66, p. 104103, 2019.
- [3] Y. Guan *et al.*, “Achieving privacy-preserving discrete fréchet distance range queries,” *IEEE Trans. Dependable Secure Comput.*, vol. 20, no. 3, pp. 2097–2110, 2023.
- [4] L. Harn *et al.*, “Lightweight aggregated data encryption for wireless sensor networks (WSNs),” *IEEE Sensors Lett.*, vol. 5, no. 4, pp. 1–4, 2021.
- [5] A. Ferdowsi *et al.*, “Deep learning-based dynamic watermarking for secure signal authentication in the Internet of Things,” in *2018 IEEE International Conference on Communications (ICC)*, 2018, pp. 1–6.
- [6] Y. Cheng *et al.*, “On information resolution of radar systems,” *IEEE Trans. Aerosp. Electron. Syst.*, vol. 48, no. 4, pp. 3084–3102, 2012.
- [7] M. S. Haynes *et al.*, “Angular and radial sampling criteria for monostatic and bistatic radar tomography of solar system small bodies,” *Adv. Space Res.*, vol. 68, no. 9, pp. 3903–3924, 2021.
- [8] B. Vandersmissen *et al.*, “Indoor person identification using a low-power FMCW radar,” *IEEE Trans. Geosci. Remote Sens.*, vol. 56, no. 7, pp. 3941–3952, 2018.
- [9] S. Mittal *et al.*, “Pedestrian detection and tracking using deformable part models and Kalman filtering,” in *2012 International SoC Design Conference (ISOCC)*, 2012, pp. 324–327.
- [10] D. P. Fairchild *et al.*, “Multistatic micro-Doppler radar for determining target orientation and activity classification,” *IEEE Trans. Aerosp. Electron. Syst.*, vol. 52, no. 1, pp. 512–521, 2016.
- [11] T. Peken *et al.*, “Blind channel estimation for massive MIMO,” *Analog Integr. Circuits Signal Process.*, vol. 91, pp. 257–266, 2017.
- [12] B. R. Mahafza, *Radar systems analysis and design using MATLAB*. Chapman and Hall/CRC, 2005.
- [13] 3GPP, “Study on channel model for frequencies from 0.5 to 100 GHz,” 3rd Generation Partnership Project (3GPP), Tech. Rep. TR 38.901, Mar. 2022.
- [14] Q.-D. Ho *et al.*, *Requirements and Regulations in the 5GHz Unlicensed Spectrum*. Cham: Springer International Publishing, 2017.